Model Difference in the Effect of Cilostazol on the Development of Experimental Pulmonary Hypertension in Rats

Toshikazu Ito (i-toshikazu@clin.medic.mie-u.ac.jp)
Mie University School of Medicine

Erquan Zhang
Fuzhou Children's Hospital of Fujian Province affiliated to Fujian Medical University

Ayaka Omori
Anesthesiology and Critical Care Medicine,Mie University School of Medicine

Jane Kabwe
Anesthesiology and Critical Care Medicine,Mie University School of Medicine

Masako Kawai
Faculty of Health,Suzuka University of Medical Science

Junko Maruyama
Faculty of Health,Suzuka University of Medical Science

Amphone Okada
Anesthesiology and Critical Care Medicine,Mie University School of Medicine

Ayumu Yokochi
Anesthesiology and Critical Care Medicine,Mie University school of Medicine

Hirofumi Sawada
Pediatrics,Mie University School of Medicine

Yoshihide Mitani
Pediatrics,Mie University School of Medicine

Kazuo Maruyama
Anesthesiology of Critical Care Medicine,Mie University School of medicine

Research article

Keywords: monocrotaline, chronic hypoxia, cilostazol, pulmonary hypertension, nitric oxide

Posted Date: February 12th, 2021

DOI: https://doi.org/10.21203/rs.3.rs-228016/v1

Version of Record: A version of this preprint was published at BMC Pulmonary Medicine on November 20th, 2021. See the published version at https://doi.org/10.1186/s12890-021-01710-4.

Abstract

Background: Preventing pulmonary vascular remodeling is a key strategy for pulmonary hypertension (PH). Causes of PH include pulmonary vasoconstriction and inflammation. This study aimed to determine whether cilostazol (CLZ), a phosphodiesterase-3 inhibitor, prevents monocrotaline (MCT)- and chronic hypoxia (CH)-induced PH development in rats.

Methods: Fifty-one male Sprague-Dawley rats were fed rat chow with (0.3% CLZ) or without CLZ for 21 days after a single injection of MCT (60 mg/kg) or saline. Forty-eight rats were fed rat chow with and without CLZ for 14 days under ambient or hypobaric (air at 380 mmHg) CH exposure. Mean PAP (mPAP), the right ventricle weight-to-left ventricle+septum weight ratio (RV/LV+S), percentages of muscularized peripheral pulmonary arteries (%Muscularization) and medial wall thickness of small muscular arteries (%MWT) were assessed.

Protein expression of endothelial nitric oxide synthase (eNOS), phosphorylated eNOS (peNOS), AKT, pAKT and IκB in lung tissue was measured by Western blotting. Monocyte chemotactic protein (MCP)-1 mRNA in lung tissue was also assessed.

Results: mPAP [35.1±1.7 mmHg (MCT) (n=9) vs.16.6±0.7 (control) (n=9) ($p<0.05$); 29.1±1.5 mmHg (CH) (n=10) vs. 17.5±0.5 (control) (n=10) ($p<0.05$)], RV/LV+S [0.40±0.01 (MCT) (n=18) vs. 0.24±0.01 (control) (n=10) ($p<0.05$); 0.41±0.03 (CH) (n=13) vs. 0.27±0.06 (control) (n=10) ($p<0.05$)], and %Muscularization and %MWT were increased by MCT injection and CH exposure. CLZ significantly attenuated these changes in the MCT model [mPAP 25.1±1.1 mmHg (n=11) ($p<0.05$), RV/LV+S 0.30±0.01 (n=14) ($p<0.05$)]. In contrast, these CLZ effects were not observed in the CH model. Lung eNOS protein expression was unchanged in the MCT model and high in the CH model. Lung protein expression of AKT, phosphorylated AKT, and IκB was downregulated by MCT, which was attenuated by CLZ; the CH model did not change these proteins. Lung MCP-1 mRNA levels were increased in MCT rats but not CH rats.

Conclusion: We found model differences in the effect of CLZ on PH development. CLZ might have a preventable effect on PH development in an inflammatory PH model but not in a vascular structural change model of PH preceded by vasoconstriction. Thus, the preventive effect of CLZ on PH development might be dependent on PH etiology.

Background

Pulmonary hypertension (PH) is characterized by an increase in pulmonary artery pressure (PAP), right ventricular hypertrophy (RVH), and functional and/or structural vascular changes [1, 2]. Possible causes of PH include pulmonary vasoconstriction, diffuse micro-thromboembolism, and pulmonary vascular remodeling [1, 2, 3]. In all conditions causing PH in humans [3, 4, 5] and experimental models [6, 7, 8, 9, 10, 11, 12, 13, 14, 15, 16], vascular changes include new muscularization of normally nonmuscular peripheral pulmonary arteries and medial hypertrophy of muscular arteries. PH may be encountered in the intensive care unit in patients with acute respiratory distress syndrome (ARDS) [17, 18, 19], congenital

heart disease with left-to-right shunt [3, 20, 21], mitral valve disease [22], and interstitial pulmonary fibrosis [23], as well as after cardiothoracic surgery [24, 25]. In all conditions causing PH, including ARDS in patients [4, 5] and experimental rat models such as monocrotaline (MCT)-induced PH [6, 12, 13, 26, 27, 28, 29, 36] and chronic hypoxia-induced PH [6, 7, 8, 9, 30, 31], vascular remodeling involves new muscularization of normally nonmuscular peripheral pulmonary arteries and medial hypertrophy of muscular arteries. A total of 7.46% of critically ill patients admitted to the intensive care unit met the ARDS criteria. The prevalence of PH in these ARDS patients was as high as 46.6% [32]. Nitric oxide (NO) is a vasodilator and suppressor of smooth muscle cell proliferation [1, 2], and the bioavailability of NO is reduced in patients with PH and in experimental PH models [33, 34, 35]. We and others have shown that modulation to increase NO production ameliorates the development of PH and vascular remodeling [6, 7, 36].

Cilostazol (CLZ) is a selective phosphodiesterase-3 inhibitor that increases intracellular cyclic AMP, which inhibits platelet aggregation and induces peripheral vasodilation. The antiplatelet agent CLZ is indicated in intermittent claudication in peripheral arterial disease [37], thrombotic complications of coronary angioplasty [38] and secondary stroke prevention [39]. Through cAMP-dependent and cAMP-independent mechanisms, CLZ also causes phosphorylation of eNOS, which increases NO production in the aortas of diabetic rats [40], human aortic endothelial cells [41], and rat cultured smooth muscle cells [42]. CLZ also has anti-inflammatory effects [43, 44, 45]. Through activating the NO synthase-NO pathway or preventing inflammatory responses, CLZ might prevent the development of PH, as suggested in an earlier study [46] in which PH was not fatal. Since the pathogenesis and severity of PH are heterogeneous [1, 2, 3, 47], we determined the effect of CLZ on the development of two established experimental models of PH: MCT-induced PH rats [6, 12, 13, 14, 15, 36, 46, 48, 49, 50, 51, 52, 53] and chronic hypoxia (CH)-induced PH rats [6, 7, 8, 9, 10, 11, 34, 35, 54, 55]. The MCT-induced PH rats in this study were used as experimental fatal PH.

Methods

The Animal Experiment Committee of Mie University School of Medicine approved the study protocol (No. 20-34 and 20-35). All the animals were housed in climate-controlled conditions with 12 h light and 12 h dark cycle. Rats were fed rat chow containing 0.3% CLZ [56] or control chow without CLZ. Rat chow with and without CLZ was a gift from Otsuka Pharmaceutical Co., Ltd (Japan). 181 Seven-week-old male healthy male Sprague-Dawley rats weighing 185–245 g were purchased from Japan SLC, Inc. The rats were anesthetized with pentobarbital, placed on a ventilator, and euthanized by incising the abdominal aorta and exsanguination.

Animal groups

MCT21 model

Seven-week-old male Sprague-Dawley rats (SLC, Japan) weighing 185-245 g were used. Rats were fed rat chow with or without CLZ one day before a single injection of MCT (60 mg/kg, Sigma) or saline and continued to be fed the same rat chow for another 21 days (Figure 1A). Each animal was randomly assigned to one of four groups: 1) a single injection of saline and rat chow without CLZ (Sal21/CLZ-) (n=10), 2) a single injection of saline and rat chow with CLZ (Sal21/CLZ+) (n=9), 3) a single injection of MCT and rat chow without CLZ (MCT21/CLZ-) (n=18), and 4) a single injection of MCT and rat chow with CLZ (MCT21/CLZ+) (n=14). MCT (60 mg/kg) [12,13,14,15,48,51,53] or the same volume of 0.9% NaCl was subcutaneously injected into the hind flank.

CH model

Seven-week-old male Sprague-Dawley rats (SLC, Japan) weighing 187-235 g were used. Rats were fed rat chow with or without CLZ beginning one day before the start of hypobaric CH exposure (air at 380 mmHg) and continued to be fed the same rat chow until the final day of ambient air or CH exposure (Figure 2A). Each animal was randomly assigned to one of four groups: 1) rats exposed to ambient air without CLZ (Air/CLZ-) (n=10), 2) rats exposed to ambient air with CLZ, (Air/CLZ+) (n=10), 3) rats exposed to CH without CLZ (CH/CLZ-) (n=14) and 4) rats exposed to CH with CLZ (CH/CLZ+) (n=14). Rats were exposed to hypoxia for 14 days and returned to ambient air after catheterization [6,8,9,10,11].

MCT28 model

In the MCT28 model, each animal injected with saline or MCT (60 mg/kg) was randomly assigned to one of three groups (Figure 1B): Sal28/CLZ- (n=5), MCT28/CLZ- (n=8), and MCT28/CLZ+ (n=9). Rats were fed for 28 days after the injection of MCT as in the MCT21 model. In the MCT28 model, the rats were used to evaluate systolic right ventricular pressure (sRVP) under 45 mg/kg pentobarbital anesthesia and RVH and to obtain lung samples for protein and mRNA assays (Figure 1B). In the MCT21 and CH models, the rats were used to evaluate awake mean PAP (mPAP), RV/LV+S, and pulmonary vascular structural changes and to obtain lung samples for protein and mRNA assays (Figures 1A, 2A).

mPAP in MCT21 and CH, and sRVP in MCT28

At the end of 21 days after the MCT injection and 14 days of CH exposure, a pulmonary artery catheter (silastic tubing, 0.31 mm ID and 0.64 mm OD) was inserted via the right external jugular vein into the pulmonary artery by employing a closed-chest technique under 45 mg/kg pentobarbital anesthesia with no tail movement with stimulation [10,11,13] (Figures 1A, 2A). The left internal carotid artery was also cannulated. Twenty-four hours after the catheterization with the rat fully conscious, the mPAP and mean artery pressure (mAP) were recorded with a physiological transducer and an amplifier system (AP 620G, Nihon Kohden, Japan) once the rats were calm (Figures 1A, 2A).

In the MCT28 model, at the end of 28 days after MCT injection, sRVP was measured by the closed-chest technique under 45 mg/kg pentobarbital anesthesia, and then lung samples for protein and mRNA assays were obtained (Figure 1B).

Preparation of lung tissue for morphometric analysis and lung sampling for protein and mRNA assays

After the measurement of awake mPAP in the MCT21 and CH models, the rats were anesthetized with 50 mg/kg pentobarbital again and mechanically ventilated through tracheostomy. The abdomen was then incised, and the abdominal aorta was incised to cause blood loss and euthanasia. A midline sternotomy was performed to expose the heart and lung. The hilum of the right lung was ligated, and the right lung was excised and put into liquid nitrogen for real-time polymerase chain reaction (PCR) and Western blotting of whole lung tissue. Blood samples were collected for hematocrit measurement. A left lung section was prepared for morphometric analysis of the vasculature using the barium injection method [6,8,9,10,11,12,13,14] to identify peripheral pulmonary arteries. Briefly, the left pulmonary artery was injected with a hot radiopaque barium-gelatin mixture at 100 cm H2O pressure [6,8,9,10,11,12,13,14]. After injection, the lung was distended and perfused through the tracheal tube with 10% formalin at 36 cm H2O pressure for 72 hr. Sections were stained for elastin by the Van Gieson method. The right ventricle (RV) of the heart was dissected from the left ventricle plus septum (LV+S) and weighed separately. The heart weight ratio (RV/LV+S) was calculated to assess RVH. Lung sampling for MCT28 was described above.

Morphometric analysis of pulmonary arteries

Light microscope slides were analyzed without previous knowledge of the treatment groups. All barium-filled arteries in each tissue section were examined at x 400, for an average of 220 arteries per section (110-340 arteries per section). Each artery was identified as being one of two structural types for the presence of muscularity: muscularized (with a complete medial coat, incomplete medial coat, or only a crescent of muscle being present) and nonmuscular (no muscle apparent) [6,8,9,10,11,12,13,14]. The percentages of muscularized arteries (%Muscularization) in peripheral pulmonary arteries with an external diameter between 15 and 50 μm and those between 51 and 100 μm were calculated. For muscular

arteries between 51 and 100 μm in diameter and those between 101 and 200 μm in diameter (an average of 18 arteries (5-20 arteries) were found per section), the wall thickness of the media (distance between external and internal elastic laminae) was measured along the shortest curvature, and the percent medial wall thickness (%MWT) was calculated [6,8,9,10,11,12,13,14].

Western blotting for eNOS, peNOS, AKT, IκB, and HMGB-1.

For Western blotting, lung samples were randomly selected from the MCT21, MCT28, and CH models, where all pooled lung samples could not be used because of the number of gel lanes. Samples were homogenized, and the supernatant was standardized to 3.0 mg/ml. Thirty micrograms of total protein from each sample was subjected to SDS-PAGE on 10% polyacrylamide gels (Nacalai, Japan) and blotted onto a PVDF membrane (Amersham Hybond-P^{R}, GE Healthcare). Blots were blocked for 1 hr in 5% skimmed milk diluted in 0.1% TBST (Tris Buffered Saline Tween) followed by incubation overnight at 4°C in primary antibody diluted in Can Get Signal Immunoreaction Enhancer Solution 1 (Toyobo Co. Ltd., Japan). Six different primary antibodies were used, including endothelial nitric oxide synthase (eNOS) (BD Transduction Laboratories; G10296, lot 21527, 1:4000 dilution), phosphorylated eNOS (peNOS) (Cell Signaling; phospho-eNOS, ser-1177 #9751, 1:2000 dilution), serine-threonine protein kinase (AKT) (Cell Signaling; #4814S, 1:2000 dilution), phosphorylated AKT (pAKT) (Cell Signaling; #460P, 1:2000 dilution), IκB-α (Cell Signaling; #4814S, 1:2000 dilution), high-mobility group box-1 (HMGB1) (Cell Signaling; #3935S, 1:2000 dilution), and beta-actin (Sigma; A5441, 1:200,000 dilution). Next, the blots were incubated in secondary antibody (Amersham NA 931, 1:20,000 dilution) diluted in Can Get Signal Immunoreaction Enhancer Solution 2 (Toyobo Co. Ltd., Japan) for 1 hr at room temperature and in Immobilon Western Chemiluminescent HRP Substrate (Millipore Corporation, USA) for 5 min. Luminescent signals were captured digitally, and densitometry was performed using Multi Gauge Ver. 3.0 (Fujifilm, Science Laboratory 2005, Japan). Each target protein was normalized to β-actin, and the relative fold change compared to the control group (100%) was calculated.

cDNA preparation and PCR

eNOS, AKT, and monocyte chemotactic protein-1 (MCP-1) mRNA levels in whole lung tissue were determined by real-time PCR. After the extraction of total RNA from whole lung tissue using TRIzol reagent (Invitrogen, USA), cDNA synthesis was performed with ReverTra Ace (Toyobo Co., Ltd., Biochemical Operations Department, Osaka, Japan). cDNA samples (15 ng of total RNA) were amplified with a StepOne Plus Real Time PCR System (Applied Biosystems). The sequences of the primer pairs are

listed in Table 1. Relative quantification was performed with the comparative ΔΔCt method by normalization to β-actin mRNA.

Survival experiment

Sixty rats (7-week-old male Sprague-Dawley rats (SLC, Japan)) were used. Each rat was randomly assigned to one of two groups: 30 rats (weighing 213-234 g) fed rat chow without CLZ and 30 rats (195-233 g) fed rat chow with CLZ (Figure 2B). The rat chow with CLZ (including 0.3% CLZ) was the same as that used with the MCT21, MCT28, and CH models. One day after the assignment of the feeding group, all rats were subcutaneously injected with MCT (60 mg/kg). Food and water were provided ad libitum. The number of rats alive was counted every day, and the Kaplan-Meier survival curve was obtained until 30 days after the injection of MCT.

Data analysis

Values are expressed as the means ± SE. When more than two means were compared, one-way analysis of variance was used. When significant variance was found, Fisher's protected least significant difference test was employed to establish which groups were different. Survival was evaluated by the Breslow-Gehan-Wilcoxon test in StatView5.0^{R}. Differences were considered significant at $P<0.05$.

Results

Body weight

MCT21 model

All rats gained body weight steadily. MCT rats had significantly lower body weights than saline control rats from day 4 to the last day of the experiment. CLZ had no effects on body weight gain in either the MCT or saline control rats (Figure 3A).

CH model

CH rats lost weight during the first several days of hypoxia exposure but regained weight afterward. The air rats gained weight steadily. After the start of hypoxia exposure, CH rats showed significantly lower body weights than air rats. CLZ treatment had no effect on the body weight of either air or CH rats (Figure 3B).

Dosage of CLZ

MCT model

Approximate dosages (mg) of CLZ were calculated by the equation food intake (g) x 0.003 x 1000, which is the average dosage per kg per day throughout the experimental course. The dosage of CLZ was ~230 mg/kg/day in the Sal/CLZ+ group and ~200 mg/kg/day in the MCT/CLZ+ group (Figure 4A). Although the dosage decreased to 64 mg/kg/day on the day of MCT injection, the dosage was similar in the Sal/CLZ+ and MCT/CLZ+ groups from day 4 throughout the experiment.

CH model

The dosage of CLZ was ~250 mg/kg/day in the air/CLZ+ group and ~220 mg/kg/day in the CH/CLZ+ group (Figure 4B). Although the dosage decreased to 11 mg/kg/day on the first day of hypoxia exposure, the dosage was similar in the Air/CLZ+ and CH/CLZ+ groups from day 4 throughout the experiment.

mPAP and RV/LV+S, mPAP/mAP and sRVP

MCT21 model

Comparing the effects of MCT administration between Sal21/CLZ- and MCT21/CLZ-, mPAP [16.56±0.73 (n=9) vs. 35.33±1.67 (n=9) mmHg ($p<0.05$) (Fig 5A)], mPAP/mAP [0.16±0.01 (n=8) vs. 0.38±0.01 (n=8) ($P<0.05$) (Fig 5B)], and RV/LV+S [0.24±0.01 (n=10) vs. 0.40±0.01 (n=18) ($P<0.05$) (Fig 5C)] were all significantly higher in MCT21/CLZ-, suggesting that MCT caused PH and RVH. Comparing the effects of CLZ treatment between MCT21/CLZ+ and MCT21/CLZ-, mPAP [25.09±1.06 (n=11) ($P<0.05$)], mPAP/mAP [0.25±0.01 (n=11)], and RV/LV+S [0.30±0.01 (n=14)] in MCT21/CLZ+ were significantly lower than those in MCT21/CLZ- (Fig. 5A, C, E), suggesting that CLZ treatment ameliorated the development of PH and RVH.

MCT28 model

Comparing the effects of MCT administration between Sal28/CLZ- and MCT28/CLZ-, sRVP and RV/LV+S was significantly higher in MCT28/CLZ-: sRVP, 30.20±3.35 (n=3) vs. 76.63±3.20 (n=8) mmHg ($p<0.05$) (Fig 6A); RV/LV+S, 0.28±0.02 (n=5) vs. 0.63±0.04 (n=8) ($P<0.05$) (Fig 6B). Comparing the effects of CLZ treatment between MCT28/CLZ+ and MCT28/CLZ-, sRVP [35.28±1.90 (n=8) ($P<0.05$) (Fig 6A)] and RV/LV+S [0.32±0.04 (n=9) ($P<0.05$)] in MCT28/CLZ+ were significantly lower than those in MCT28/CLZ- (Fig. 6B), suggesting again that CLZ treatment ameliorated the development of PH and RVH.

CH model

CH caused PH with a mPAP of 29.1±1.5 mmHg (n=10) (CH/CLZ-) compared to that in Air/CLZ- 17.5±0.5 mmHg (n=10) ($p<0.05$). There were no significant differences between CH/CLZ+ and CH/CLZ- individuals (Figure 5B). RV/LV+S was higher in CH/CLZ- 0.41±0.03 (n=13) than in Air/CLZ- 0.27±0.06 (n=10) ($p<0.05$). There were no significant differences in RV/LV+S between CH/CLZ+ and CH/CLZ- (Figure 5F). The ratio of mPAP/mAP was also higher in CH/CLZ- than Air/CLZ-, with no significant difference between CH/CLZ+ and CH/CLZ- (Figure 5D).

Survival

CLZ treatment significantly improved survival from 26 days after MCT injection in MCT-induced PH rats (Figure 7).

Vascular structural changes

MCT21 model

The %Muscularization was higher in those with external diameters between 15 and 50 μm (Figure 8A) and those between 51 and 100 μm (Figure 8B) in MCT21/CLZ- than in Sal21/CLZ-. MCT21/CLZ+ had significantly lower %Muscularization in both sizes of arteries than MCT21/CLZ- (Figure 8A, B). The %MWT in MCT21/CLZ- was higher than that in Sal21/CLZ- in the small muscular arteries between 51 and 100 μm in external diameter at the alveolar duct level, and those between 101 and 200 μm in external diameter were usually accompanied by terminal or respiratory bronchioles (Figure 8C, D). MCT21/CLZ+ had a significantly lower %MWT than MCT21/CLZ- (Figure 8C, D).

CH model

The %Muscularization (Figure 9A, B) and %MWT (Figure 9C, D) were significantly higher in CH/CLZ- than Air/CLZ-, whereas CH/CLZ+ had no significant differences compared to CH/CLZ- (Figure 9A, B, C, D).

Hematocrit

Hematocrit was similar among the Sal21/CLZ-, Sal21/CLZ+, MCT21/CLZ- and MCT21/CLZ+ groups: 43.9±0.7% (n=9), 41.4±1.4% (n=9), 41.3±1.5% (n=16), and 42.4±1.5% (n=14), respectively. Hematocrit in CH/CLZ- 56.1±1.6% (n=9) was significantly higher than in Air/CLZ- 42.8±1.7% (n=9). CH/CLZ+ 56.1±1.6% (n=11) had values similar to those of CH/CLZ-.

Western blotting and PCR

eNOS and peNOS

MCT had no effect on eNOS protein expression (Figure 10A, B), whereas CH upregulated eNOS protein expression (Figure 10C). MCT also had no effect on eNOS mRNA levels (Figure 10G, H), whereas chronic hypoxia increased eNOS mRNA expression (Figure 10I). MCT decreased peNOS protein expression (Figure 10D, E), whereas CH did not (Figure 10F). CLZ increased eNOS mRNA levels in the MCT21 group (Figure 10G) and decreased peNOS expression in the CH group (Figure 10F).

AKT and pAKT

MCT significantly downregulated AKT protein expression in the MCT21 model (Figure 11A) and pAKT protein expression in the MCT28 model (Figure 11E). CLZ significantly attenuated this decrease in pAKT protein expression in the MCT28 model (Figure 11E) and increased AKT mRNA expression in the MCT28 model (Figure 11H). In the CH model, AKT mRNA, AKT protein and pAKT expression were unchanged, and CLZ had no effect (Figure 11C, F, I).

IκB and HMGB-1

MCT downregulated IκB (Figure 12A, B) and HMGB-1 (Figure 12D, E) protein expression in both the MCT21 and MCT28 models (Figure 12A, B, D, E). CLZ significantly attenuated the downregulation of both IκB (Figure 12B) and HMGB-1 (Figure 12E) protein expression in the MCT28 model. In the CH model, IκB and HMGB-1 protein expression was unchanged, and CLZ had no effect (Figure 12C, F).

MCP-1

The mRNA expression of MCP-1 was higher in MCT21/CLZ- than in Sal21/CLZ-. There was no significant difference between MCT21/CLZ- and MCT21/CLZ+ (Figure 13A). In the MCT28 and CH models, there were no differences in MCP-1 mRNA levels among the groups (Figure 13B, C).

Discussion

The MCT and CH models were used to determine the model difference in the effect of CLZ on the development of PH. In both the MCT model and CH model, rats developed increases in mPAP and RV/LV + S, suggesting the successful development of PH. CLZ treatment ameliorated the development of MCT-induced PH. Hypertensive pulmonary vascular remodeling (i.e., new muscularization of peripheral

pulmonary arteries and medial hypertrophy of muscular arteries) in the MCT model was ameliorated by CLZ treatment. In the CH model, CLZ treatment did not ameliorate the development of PH or hypertensive vascular remodeling.

High hematocrit contributes to high PAP in the CH model in addition to hypertensive pulmonary vascular remodeling [11], where the decrease in hematocrit is expected to reduce PAP. Since the hematocrit in both the CH and MCT models was not changed by CLZ, attenuation of the mPAP by CLZ treatment was not due to the decrease in hematocrit. Medial hypertrophy of the muscular artery indicates the hypertrophy and hyperplasia of vascular smooth muscle cells, whereas new muscularization of normally nonmuscular arteries indicates the differentiation of pericytes to mature smooth muscle cells [11, 12]. Previous studies showed that increasing endogenous NO could ameliorate these structural changes [6, 36]. Earlier studies revealed that eNOS mRNA is increased in the lungs of CH-induced PH rats [54, 57], consistent with the present results. Since CLZ increases NOS expression in cultured endothelium [40, 41], we expected to observe the upregulation of NOS due to CLZ in CH lung tissue. CLZ might have no effect on NOS synthesis, at least in CH whole lung tissue, since eNOS protein levels in the lung tissue were similar between CH-induced PH rats with and without CLZ. This suggests that combined CH and CLZ treatment did not further enhance eNOS expression compared with CH-induced NOS upregulation. Although eNOS mRNA expression was increased by CLZ in the MCT21 model, which is consistent with an earlier study [46], CLZ had no effect on the protein expression of eNOS and peNOS in either model. Translation of eNOS mRNA might be impaired in the MCT model; therefore, it is difficult to explain the preventable effect of CLZ in the MCT model by increased NO production.

MCT-induced PH rats [6, 12, 13, 14, 15, 36, 46, 48, 49, 50, 51, 52, 53] have been used to investigate pulmonary vascular remodeling in inflammatory-related PH, including ARDS [4, 5]. CH-induced PH [6, 7, 8, 9, 10, 11, 34, 35, 54, 55] is a type of PH due to hypoxia that includes patients residing at high altitude and patients with chronic obstructive pulmonary disease. Endothelial injury precedes the increase in PAP in MCT-induced PH [51], whereas the increase in PAP precedes the development of vascular changes in CH-induced PH [10]. A previous study showed that chronic NO inhalation prevented the development of PH and pulmonary vascular remodeling in CH-induced PH [7] but not in MCT-induced PH [12]. NO inhalation causes selective pulmonary vasodilation. Thus, the different effects of inhaled NO between PH models suggest that reversing vasoconstriction is effective in preventing the development of PH in some forms in which vasoconstriction is the initial insult. Since CLZ could not prevent the development of CH-induced PH, we speculate that CLZ has a less potent pulmonary vasodilating effect. Endothelial injury is the initial insult in MCT-induced PH [51]. CLZ has been reported to promote endothelial regeneration in injured carotid arteries [58] and endothelial proliferation in lymphatics [59].

There are several limitations in this study. First, the present results were in adult male rats, and we must be cautious in discussing neonatal and juvenile rats and/or infant and pediatric human patients, since age and sex influence pulmonary hypertension in chronic hypoxia [60], and animal models do not completely recapture human disease [16]. Second, the dosage of CLZ was higher in the present study than in the previous study [46]. We used this concentration because chow including 0.3% CLZ was used

in spontaneously hypertensive rats [56]. The rats in the previous study [46] did not have a lethal condition compared with the rats in the present study. Third, this study is observational and not mechanistic. CLZ enhances Akt phosphorylation in human aortic endothelial cells [41] and in neuroblastoma cells [43]. In human aortic endothelial cells [41] and canine coronary blood vessels [61], PI3/AKT-dependent NO production has been reported. Since attenuation of the decrease in pAKT, an active form of AKT, was detected in the MCT model with no changes in the CH model, this effect of CLZ might partly explain the model difference in the effect of CLZ. Although one of the targets of pAKT is eNOS [61], this is not the case in the present study because we could not detect upregulation of peNOS expression.

An earlier study in our laboratory showed that MCT treatment significantly reduced the protein levels of IκBα in lung tissues, which was restored by pyrrolidine dithiocarbamate (PDTC), an NFκB inhibitor [48]. NFκB is a transcription factor that regulates the transcription of genes involved in inflammatory responses. The decrease in the protein levels of IκBα has been reported to be associated with the upregulation of NFκB activity [62]. IκBα was unchanged in CH-induced PH rats but decreased in MCT-induced PH rats in the current study, consistent with our earlier study [48], suggesting that inflammatory components play a greater role in the etiology of MCT than in the chronic hypoxia model. Increased mRNA expression of lung MCP-1 in the present study also supports the inflammatory component of the MCT model. The mechanism and role of MCP-1 in the inflammatory response are chemotactic and activating effects on monocytes/macrophages [53]. In the MCT model, we and others have shown macrophage infiltration into the alveolar wall by 14 days after MCT injection [15, 48]. The plasma and bronchoalveolar lavage fluid (BALF) MCP-1 levels increased transiently and then returned to normal levels [53]. We also showed that lung MCP-1 mRNA was elevated in MCT21 rats in the present study and showed increases in BALF MCP-1 and TNFα levels measured by ELISA in a previous study [14], suggesting the presence of inflammation in MCT rats. The anti-inflammatory effect of CLZ [43, 63] might explain the reversal of decreased levels of IκBα in the lungs of MCT-injected rats. CLZ has been reported to inactivate NFκB [64, 65]. Moreover, retinoic acid prevented the development of MCT-induced PH with the inhibition of MMP-1 [50]. NFκB induces the promotion of MMP-1 [66], and CLZ was reported to prevent MMP-1 in a cell study [67].

HMGB-1 is normally present as a nuclear protein and is passively released from damaged cells [44].

The lower expression of HMGB-1 in the lung tissue of MCT-injected rats might be due to the increased release of HMGB-1 protein into the circulation, which might reflect damage to the cells. A recent study showed that the increase in serum HMGB-1 is associated with the concurrent decrease in tissue HMGB-1 protein expression [68]. CLZ restored HMGB-1 protein expression to the control level 28 days after MCT injection, which might show an ability of CLZ to ameliorate cell damage and improve survival. Furthermore, CLZ inhibits HMGB-1 release in lipopolysaccharide-activated HMGB-1 release and increases the survival of endotoxemic mice [63].

In summary, the administration of CLZ prevented the development of PH in MCT-induced PH, although CH-induced PH development was not prevented by CLZ. The inhibitory effect of CLZ on the development

of PH might depend on the etiology of PH, in which alterations in lung AKT, pAKT, and IκB might partly be related.

Abbreviations

PH
pulmonary hypertension
CLZ
cilostazol
MCT
monocrotaline
CH
chronic (hypobaric) hypoxia
RV/LV + S
ratio of cardiac right ventricle/(left ventricle to septum)
mPAP
mean pulmonary artery pressure
mAP
mean artery pressure
sRVP
systolic right ventricular pressure
PCR
polymerase chain reaction
%Muscularization
percentages of muscularized arteries
%MWT
percent medial wall thickness
eNOS
endothelial nitric oxide synthase
AKT
serine-threonine protein kinase
MCP-1
monocyte chemotactic protein-1

Declarations

Ethics approval and consent to participate

The Animal Care and Use Committee of Mie University School of Medicine approved the research protocol (No. 20-34 and 20-35).

Consent for publication

Not applicable

Availability of data and materials

All data generated or analyzed during this study are included in this published article [and its supplementary information files].

Competing interests

The authors declare that they have no competing interests.

Funding

This work was financially supported by grants in aid for scientific research from the Japanese Ministry of Education, Science and Culture. (Grants-in-Aid 17K11075).

Authors’ contributions

TI and EZ contributed equally to this work, collecting and analyzing the data, and drafting the manuscript. AO, JK, JM, MK, and AO made substantial contributions to data acquisition and reviewing the manuscript. HS, AY, and YM contributed to the study design, statistical analysis, interpretation of data, and final approval of the manuscript. KM conceived the study, participated in its design and coordination, and helped to draft the manuscript. All authors read and approved the final manuscript.

Competing interests

We have no financial relationships to disclose.

Acknowledgment

We would like to thank Otsuka Pharmaceutical Co. for the gift of rat chow.

References

1. Archer SL, Weir EK, Wilkins MR. Basic science of pulmonary arterial hypertension for clinicians: new concepts and experimental therapies. 2010; 121:2045-66

2. Rabinovitch M. Molecular pathogenesis of pulmonary arterial hypertension. J Clin Invest. 2008; 118:2372-9.
3. Rabinovitch M, Keane JF, Norwood WI, Castaneda AR, Reid L. Vascular structure in lung tissue obtained at biopsy correlated with pulmonary hemodynamic findings after repair of congenital heart defects. 1984; 69:655-67
4. Snow RL, Davies P, Pontoppidan H, Zapol WM, Reid L. Pulmonary vascular remodeling in adult respiratory distress syndrome. Am Rev Respir Dis. 1982;126:887-92
5. Tomashefski JF Jr, Davies P, Boggis C, Greene R, Zapol WM, Reid LM. The pulmonary vascular lesions of the adult respiratory distress syndrome. Am J Pathol. 1983; 112:112-26.
6. Mitani Y, Maruyama K, Sakurai M. Prolonged administration of L-arginine ameliorates chronic pulmonary hypertension and pulmonary vascular remodeling in rats. Circulation.1997;96:689-97.
7. Kouyoumdjian C, Adnot S, Levame M, Eddahibi S, Bousbaa H, Raffestin B. Continuous inhalation of nitric oxide protects against development of pulmonary hypertension in chronically hypoxic rats. J Clin Invest. 1994; 94:578-84.
8. Zhang E, Jiang B, Yokochi A, Maruyama J, Mitani Y, Ma N, Maruyama K.Effect of all-trans-retinoic acid on the development of chronic hypoxia-induced pulmonary hypertension. Circ J. 2010; 74:1696-703
9. Zhang E, Maruyama J, Yokochi A, Mitani Y, Sawada H, Nishikawa M, Ma N, Maruyama K. Sarpogrelate hydrochloride, a serotonin 5HT2A receptor antagonist, ameliorates the development of chronic hypoxic pulmonary hypertension in rats. J Anesth. 2015; 29:715-23.
10. Rabinovitch M, Gamble W, Nadas AS, Miettinen OS, Reid L. Rat pulmonary circulation after chronic hypoxia: hemodynamic and structural features. Am J Physiol. 1979;236:H818-27
11. Maruyama K, Ye CL, Woo M, Venkatacharya H, Lines LD, Silver MM, Rabinovitch M. Chronic hypoxic pulmonary hypertension in rats and increased elastolytic activity. Am J Physiol. 1991;261:H1716-26.
12. Maruyama J, Maruyama K, Mitani Y, Kitabatake M, Yamauchi T, Miyasaka K. Continuous low-dose NO inhalation does not prevent monocrotaline-induced pulmonary hypertension in rats. Am J Physiol. 1997;272:H517-24.
13. Ilkiw R, Todorovich-Hunter L, Maruyama K, J Shin, and M Rabinovitch. SC-39026, a serine elastase inhibitor, prevents muscularization of peripheral arteries, suggesting a mechanism of monocrotaline-induced pulmonary hypertension in rats. Circ Res 1989; 64: 814-25
14. Yamada Y, Maruyama J, Zhang E, Okada A, Yokochi A, Sawada H, Mitani Y, Hayashi T, Suzuki K, Maruyama K. Effect of thrombomodulin on the development of monocrotaline-induced pulmonary hypertension. J Anesth. 2014;28:26-33.
15. Meyrick B, Gamble W, Reid L. Development of Crotalaria pulmonary hypertension: hemodynamic and structural study. Am J Physiol. 1980;239:H692-702.
16. Stenmark KR, Meyrick B, Galie N, Mooi WJ, McMurtry IF. Animal models of pulmonary arterial hypertension: the hope for etiological discovery and pharmacological cure. Am J Physiol Lung Cell

Mol Physiol. 2009;297:L1013-32.

17. Zapol WM, Snider MT. Pulmonary hypertension in severe acute respiratory failure. N Engl J Med. 1977; 296:476-80.
18. Maruyama K, Nakai Y, Takeuchi M, Mizumoto T, Chikusa H, Muneyuki M. Verapamil reduced pulmonary hypertension in adult respiratory distress syndrome. J Anesth. 1994; 8:480-1.
19. Maruyama K, Takeuchi M, Chikusa H, Muneyuki M. Reduction of intrapulmonary shunt by low-dose inhaled nitric oxide in a patient with late-stage respiratory distress associated with paraquat poisoning. Intensive Care Med. 1995;21:778-9.
20. Maruyama K, Maruyama J, Utsunomiya H, Furuhashi K, Kurobuchi M, Katayama Y, Yada I, Muneyuki M. Effect of nicardipine on pulmonary hypertension after repair of congenital heart defects in early postoperative period. J Anesth. 1993; 7:95-101.
21. Shimpo H, Mitani Y, Tanaka J, Mizumoto T, Onoda K, Tani K, Yuasa H, Yada I, Maruyama K. Inhaled low-dose nitric oxide for postoperative care in patients with congenital heart defects. Artif Organs. 1997; 21:10-3.
22. Breitling S, Ravindran K, Goldenberg NM, Kuebler WM. The pathophysiology of pulmonary hypertension in left heart disease. Am J Physiol Lung Cell Mol Physiol. 2015;309:L924-41.
23. Maruyama K, Kobayasi H, Taguchi O, Chikusa H, Muneyuki M. Higher doses of inhaled nitric oxide might be less effective in improving oxygenation in a patient with interstitial pulmonary fibrosis. Anesth Analg. 1995; 81:210-1.
24. Zamanian RT, Haddad F, Doyle RL, Weinacker AB. Management strategies for patients with pulmonary hypertension in the intensive care unit. Crit Care Med. 2007;35:2037-50.
25. Goldenberg NM, Rabinovitch M, Steinberg BE. Inflammatory Basis of Pulmonary Arterial Hypertension: Implications for Perioperative and Critical Care Medicine. Anesthesiology. 2019; 131:898-907.
26. Hill NS, Warburton RR, Pietras L, Klinger JR. Nonspecific endothelin-receptor antagonist blunts monocrotaline-induced pulmonary hypertension in rats. J Appl Physiol. 1997;83:1209-15.
27. Schermuly RT, Kreisselmeier KP, Ghofrani HA, Yilmaz H, Butrous G, Ermert L, Ermert M, Weissmann N, Rose F, Guenther A, Walmrath D, Seeger W, Grimminger F. Chronic sildenafil treatment inhibits monocrotaline-induced pulmonary hypertension in rats. Am J Respir Crit Care Med. 2004;169:39-45.
28. Dony E, Lai YJ, Dumitrascu R, Pullamsetti SS, Savai R, Ghofrani HA, Weissmann N, Schudt C, Flockerzi D, Seeger W, Grimminger F, Schermuly RT. Partial reversal of experimental pulmonary hypertension by phosphodiesterase-3/4 inhibition. Eur Respir J. 2008;31:599-610.
29. Schermuly RT, Kreisselmeier KP, Ghofrani HA, Samidurai A, Pullamsetti S, Weissmann N, Schudt C, Ermert L, Seeger W, Grimminger F. Antiremodeling effects of iloprost and the dual-selective phosphodiesterase 3/4 inhibitor tolafentrine in chronic experimental pulmonary hypertension. Circ Res. 2004;94:1101-8.
30. Eddahibi S, Raffestin B, Clozel M, Levame M, Adnot S. Protection from pulmonary hypertension with an orally active endothelin receptor antagonist in hypoxic rats. Am J Physiol. 1995;268:H828-35.

31. Zhao L, Mason NA, Morrell NW, Kojonazarov B, Sadykov A, Maripov A, Mirrakhimov MM, Aldashev A, Wilkins MR. Sildenafil inhibits hypoxia-induced pulmonary hypertension. Circulation. 2001; 104:424-8.
32. Ñamendys-Silva S.A., Santos-Martínez L.E., Pulido T. Pulmonary hypertension due to acute respiratory distress syndrome. Braz J Med Biol Res. 2014; 47: 904–910.
33. Klinger JR, Kadowitz PJ The Nitric Oxide Pathway in Pulmonary Vascular Disease. Am J Cardiol. 2017; 120: S71-9.
34. Maruyama J, Jiang BH, Maruyama K, Takata M, Miyasaka K. Prolonged nitric oxide inhalation during recovery from chronic hypoxia does not decrease nitric oxide-dependent relaxation in pulmonary arteries. 2004;126:1919-25.
35. Maruyama J, Maruyama K. Impaired nitric oxide-dependent responses and their recovery in hypertensive pulmonary arteries of rats. Am J Physiol. 1994;266:H2476-88.
36. Zhao YD, Courtman DW, Deng Y, Kugathasan L, Zhang Q, Stewart DJ. Rescue of monocrotaline-induced pulmonary arterial hypertension using bone marrow-derived endothelial-like progenitor cells: efficacy of combined cell and eNOS gene therapy in established disease. Circ Res. 2005; 96:442-50.
37. Hiatt WR. The US experience with cilostazol in treating intermittent claudication. Suppl. 2005; 6:21-31.
38. Tsuchikane E, Fukuhara A, Kobayashi T, Kirino M, Yamasaki K, Kobayashi T, Izumi M, Otsuji S, Tateyama H, Sakurai M, Awata N. Impact of cilostazol on restenosis after percutaneous coronary balloon angioplasty. 1999; 100:21-6
39. Noma K, Higashi Y. Cilostazol for treatment of cerebral infarction. Expert Opin Pharmacother. 2018; 19:1719-26.
40. Suzuki K, Uchida K, Nakanishi N, Hattori Y. Cilostazol activates AMP-activated protein kinase and restores endothelial function in diabetes. Am J Hypertens. 2008; 21:451-7.
41. Hashimoto A, Miyakoda G, Hirose Y, Mori T. Activation of endothelial nitric oxide synthase by cilostazol via a cAMP/protein kinase A- and phosphatidylinositol 3-kinase/Akt-dependent mechanism. Atherosclerosis. 2006; 189:350-7.
42. Ikeda U, Ikeda M, Kano S, Kanbe T, Shimada K. Effect of cilostazol, a cAMP phosphodiesterase inhibitor, on nitric oxide production by vascular smooth muscle cells. Eur J Pharmacol. 1996; 314:197-202.
43. Hassan M, Ibrahim MA, Hafez HM, Mohamed MZ, Zenhom NM, Abd Elghany HM. Role of Nrf2/HO-1 and PI3K/Akt Genes in the Hepatoprotective Effect of Cilostazol. Curr Clin Pharmacol. 2019; 14:61-7.
44. Andersson U, Tracey KJ. HMGB1 is a therapeutic target for sterile inflammation and infection. Annu Rev Immunol. 2011; 29:139-62.
45. Sakamoto T, Ohashi W, Tomita K, Hattori K, Matsuda N, Hattori Y. Anti-inflammatory properties of cilostazol: Its interruption of DNA binding activity of NF-κB from the Toll-like receptor signaling pathways. Int Immunopharmacol. 2018;62:120-31.

46. Chang LT, Sun CK, Sheu JJ, Chiang CH, Youssef AA, Lee FY, Wu CJ, Yip HK. Cilostazol therapy attenuates monocrotaline-induced pulmonary arterial hypertension in rat model. Circ J. 2008; 72:825-31.
47. Simonneau G, Gatzoulis MA, Adatia I, Celermajer D, Denton C, Ghofrani A, Gomez Sanchez MA, Krishna Kumar R, Landzberg M, Machado RF, Olschewski H, Robbins IM, Souza R. Updated clinical classification of pulmonary hypertension. J Am Coll Cardiol. 2013; 62: D34-41.
48. Sawada H, Mitani Y, Maruyama J, Jiang BH, Ikeyama Y, Dida FA, Yamamoto H, Imanaka-Yoshida K, Shimpo H, Mizoguchi A, Maruyama K, Komada Y. A nuclear factor-kappaB inhibitor pyrrolidine dithiocarbamate ameliorates pulmonary hypertension in rats. Chest. 2007; 132:1265-74
49. Dai M, Xiao R, Cai L, Ge T, Zhu L, Hu Q. HMGB1 is mechanistically essential in the development of experimental pulmonary hypertension. Am J Physiol Cell Physiol. 2019;316:C175-85.
50. Qin Y, Zhou A, Ben X, et al. All-trans retinoic acid in pulmonary vascular structural remodeling in rats with pulmonary hypertension induced by monocrotaline. Chinese Med J. 2001; 114: 462-5.
51. Rosenberg HC, Rabinovitch M. Endothelial injury and vascular reactivity in monocrotaline pulmonary hypertension. Am J Physiol. 1988; 255:H1484-91
52. Voelkel NF, Tuder RM, Bridges J, Arend WP. Interleukin-1 receptor antagonist treatment reduces pulmonary hypertension generated in rats by monocrotaline. Am J Respir Cell Mol Biol. 1994;11:664-75.
53. Kimura H, Kasahara Y, Kurosu K, Sugito K, Takiguchi Y, Terai M, Mikata A, Natsume M, Mukaida N, Matsushima K, Kuriyama T. Alleviation of monocrotaline-induced pulmonary hypertension by antibodies to monocyte chemotactic and activating factor/monocyte chemoattractant protein-1. Lab Invest. 1998;78:571-81.
54. Le Cras TD, Xue C, Renqasamy A, et al. Chronic hypoxia upregulates endothelial and inducible NO synthase gene and protein expression in rat lung. Am J Physiol 1996; 270: L164-170
55. Yokochi A, Itoh H, Maruyama J, Zhang E, Jiang B, Mitani Y, Hamada C, Maruyama K. Colforsin-induced vasodilation in chronic hypoxic pulmonary hypertension in rats. J Anesth. 2010;24:432-40.
56. Otsuka Pharmaceutical Co. LTD. Standard Commondity Classification Number of Japan 873399. PLETAAL^{R} OD Tablets 50mg・100mg, Medical attachment, HD89D2B01, 2019
57. Tyler RC, Muramatsu M, Abman SH, et al. Variable expression of endothelial NO synthase in three forms of rat pulmonary hypertension. Am J Physiol 1999; 276: L297-303
58. Kawabe-Yako R, Ii M, Masuo O, Asahara T, Itakura T. Cilostazol activates function of bone marrow-derived endothelial progenitor cell for re-endothelialization in a carotid balloon injury model. PLoS One. 2011;6:e24646.
59. Kimura T, Hamazaki TS, Sugaya M, Fukuda S, Chan T, Tamura-Nakano M, Sato S, Okochi H. Cilostazol improves lymphatic function by inducing proliferation and stabilization of lymphatic endothelial cells. J Dermatol Sci. 2014;74:150-8.

60. Rabinovitch M, Gamble WJ, Miettinen OS, Reid L. Age and sex influence on pulmonary hypertension of chronic hypoxia and on recovery. Am J Physiol. 1981;240:H62-72.
61. Zhang XP, Hintze TH. cAMP signal transduction induces eNOS activation by promoting PKB phosphorylation. Am J Physiol Heart Circ Physiol. 2006;290:H2376-84.
62. Beg AA, Finco TS, Nantermet PV, Baldwin AS Jr. Tumor necrosis factor and interleukin-1 lead to phosphorylation and loss of I kappa B alpha: a mechanism for NF-kappa B activation. Mol Cell Biol. 1993;13:3301-10
63. Chang KC. Cilostazol inhibits HMGB1 release in LPS-activated RAW 264.7 cells and increases the survival of septic mice. Thromb Res. 2015;136:456-64.
64. Jung WK, Lee DY, Park C, Choi YH, Choi I, Park SG, Seo SK, Lee SW, Yea SS, Ahn SC, Lee CM, Park WS, Ko JH, Choi IW. Cilostazol is anti-inflammatory in BV2 microglial cells by inactivating nuclear factor-kappaB and inhibiting mitogen-activated protein kinases. Br J Pharmacol. 2010;159:1274-85.
65. Park WS, Jung WK, Lee DY, Moon C, Yea SS, Park SG, Seo SK, Park C, Choi YH, Kim GY, Choi JS, Choi IW. Cilostazol protects mice against endotoxin shock and attenuates LPS-induced cytokine expression in RAW 264.7 macrophages via MAPK inhibition and NF-kappaB inactivation: not involved in cAMP mechanisms. Int Immunopharmacol. 2010;10:1077-85.
66. O'Kane CM, Elkington PT, Jones MD, Caviedes L, Tovar M, Gilman RH, Stamp G, Friedland JS. STAT3, p38 MAPK, and NF-kappaB drive unopposed monocyte-dependent fibroblast MMP-1 secretion in tuberculosis. Am J Respir Cell Mol Biol. 2010;43:465-74.
67. Yu BC, Lee DS, Bae SM, Jung WK, Chun JH, Urm SH, Lee DY, Heo SJ, Park SG, Seo SK, Yang JW, Choi JS, Park WS, Choi IW. The effect of cilostazol on the expression of matrix metalloproteinase-1 and type I procollagen in ultraviolet-irradiated human dermal fibroblasts. Life Sci. 2013;92:282-8.
68. Nakamura K, Hatano E, Miyagawa-Hayashino A, Okuno M, Koyama Y, Narita M, Seo S, Taura K, Uemoto S. Soluble thrombomodulin attenuates sinusoidal obstruction syndrome in rat through suppression of high mobility group box 1. Liver Int. 2014;34:1473-87. Liver Int. 2014;34:1473-87.

Tables

Due to technical limitations, table 1 is only available as a download in the Supplemental Files section.

Figures

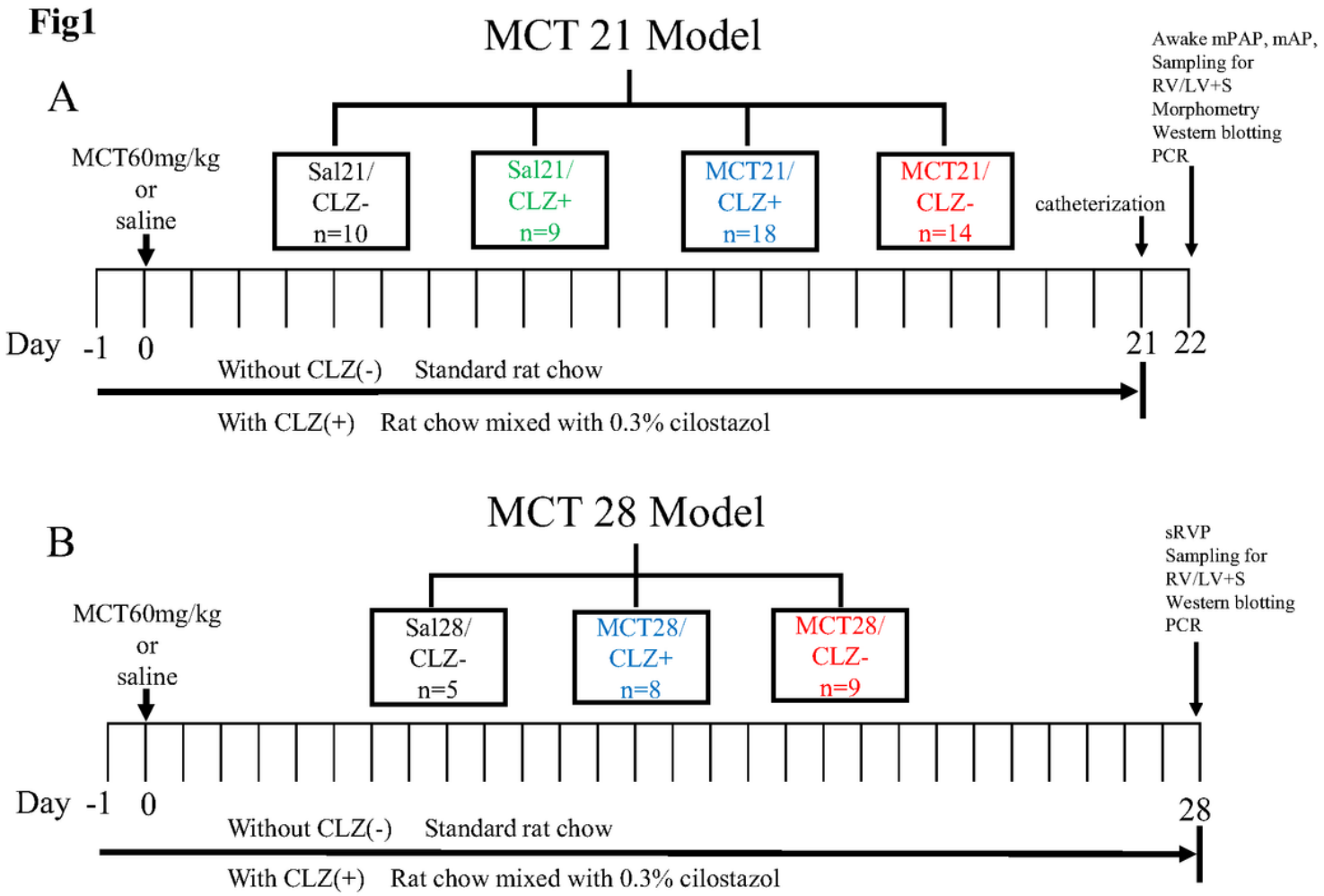

Figure 1

Experimental protocol of MCT21 and MCT28 models A, MCT21 model: catheterization of pulmonary and carotid arteries was performed 21 days after the MCT or saline injection; awake mean pulmonary artery pressure (mPAP) and mean artery pressure (mAP) were measured at day 22 with rats fully awake; lung and heart samples were obtained for right ventricle (RV) weight-to-left ventricle+septum (LV+S) weight ratio (RV/LV+S), morphometry of pulmonary arteries, Western blotting and PCR after the pressure measurements. B, MCT28 model: systolic right ventricular pressure (sRVP) under anesthesia and sampling for RV/LV+S. Western blotting and PCR were performed 28 days after the injection of MCT or saline. Sal/CLZ-, rats injected with saline and fed rat chow without cilostazol (CLZ) Sal/CLZ+, rats injected with saline and fed rat chow with CLZ MCT/CLZ-, rats injected with MCT and fed rat chow without CLZ MCT/CLZ+, rats injected with MCT and fed rat chow with CLZ MCT, monocrotaline; Sal, saline; n=, number of rats used. We could not always succeed in obtaining all these data sets or samples for each assigned rat because of technical reasons, especially in taking mPAP, so the number of rats used (n) was not always the same as the number in Figures 5, 6, 8, and 9.

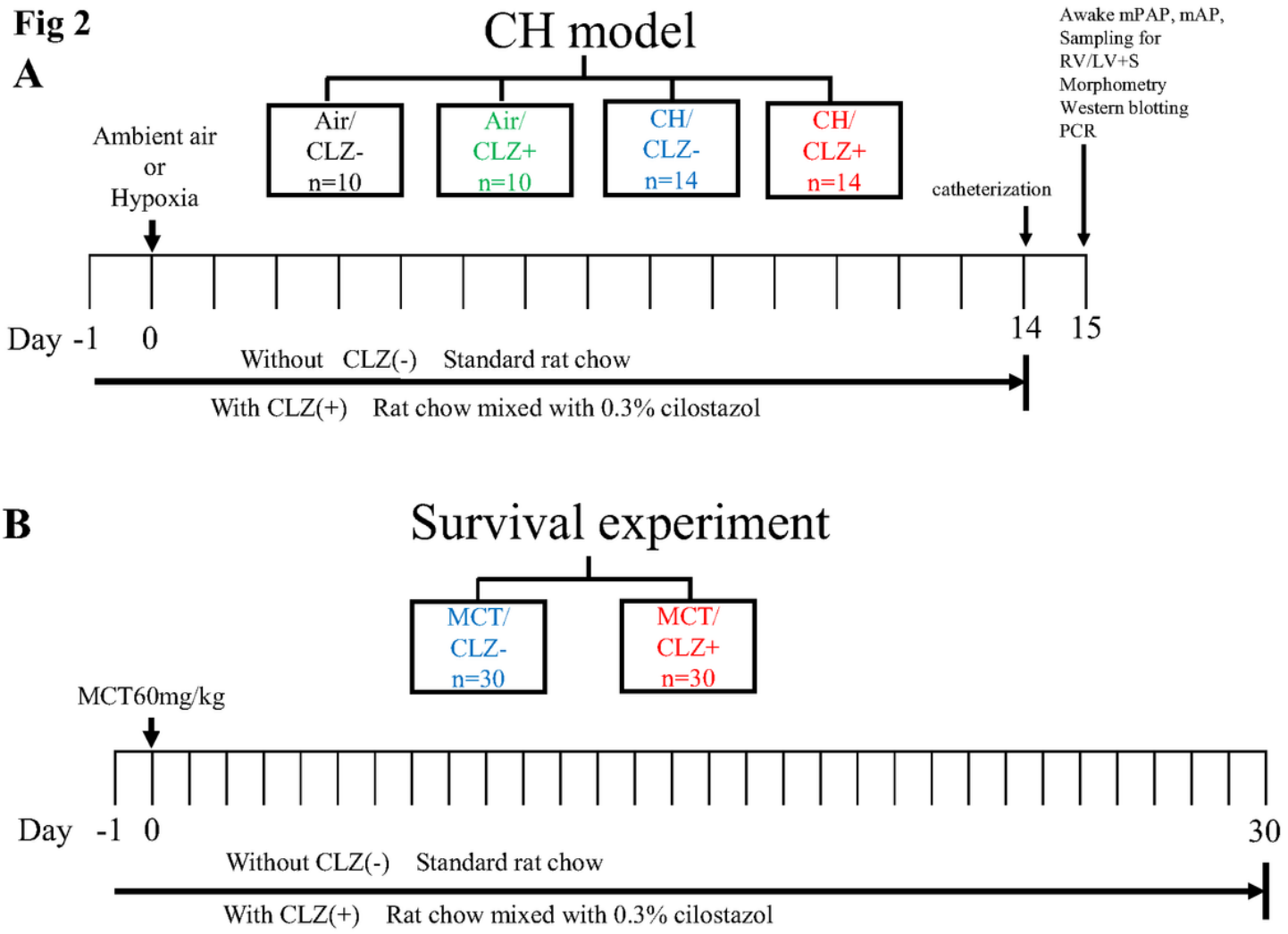

Figure 2

Experimental protocol of CH model and survival study A, CH model: catheterization of pulmonary and carotid arteries was performed on the final day of chronic hypoxia (CH) exposure; awake mean pulmonary artery pressure (mPAP) and mean artery pressure (mAP) were measured on day 15 with rats fully awake; lung and heart samples were obtained for right ventricle weight-to-left ventricle+septum weight ratio (RV/LV+S), morphometry of pulmonary arteries, Western blotting and PCR after the pressure measurements. Air/CLZ-, rats exposed to ambient air and fed rat chow without CLZ Air/CLZ+, rats exposed to ambient air and fed rat chow with CLZ CH/CLZ-, rats exposed to chronic hypoxia and fed rat chow without CLZ CH/CLZ+, rats exposed to chronic hypoxia and fed rat chow with CLZ n=, number of rats used. The number of rats used (n) was not always the same as the number in Figures 5, 6, 8, and 9. See the legend of Figure 1. B, Survival experiment. MCT/CLZ-, rats injected with MCT and fed rat chow without CLZ MCT/CLZ+, rats injected with MCT and fed rat chow with CLZ MCT, monocrotaline; Sal, saline; N=, number of rats used.

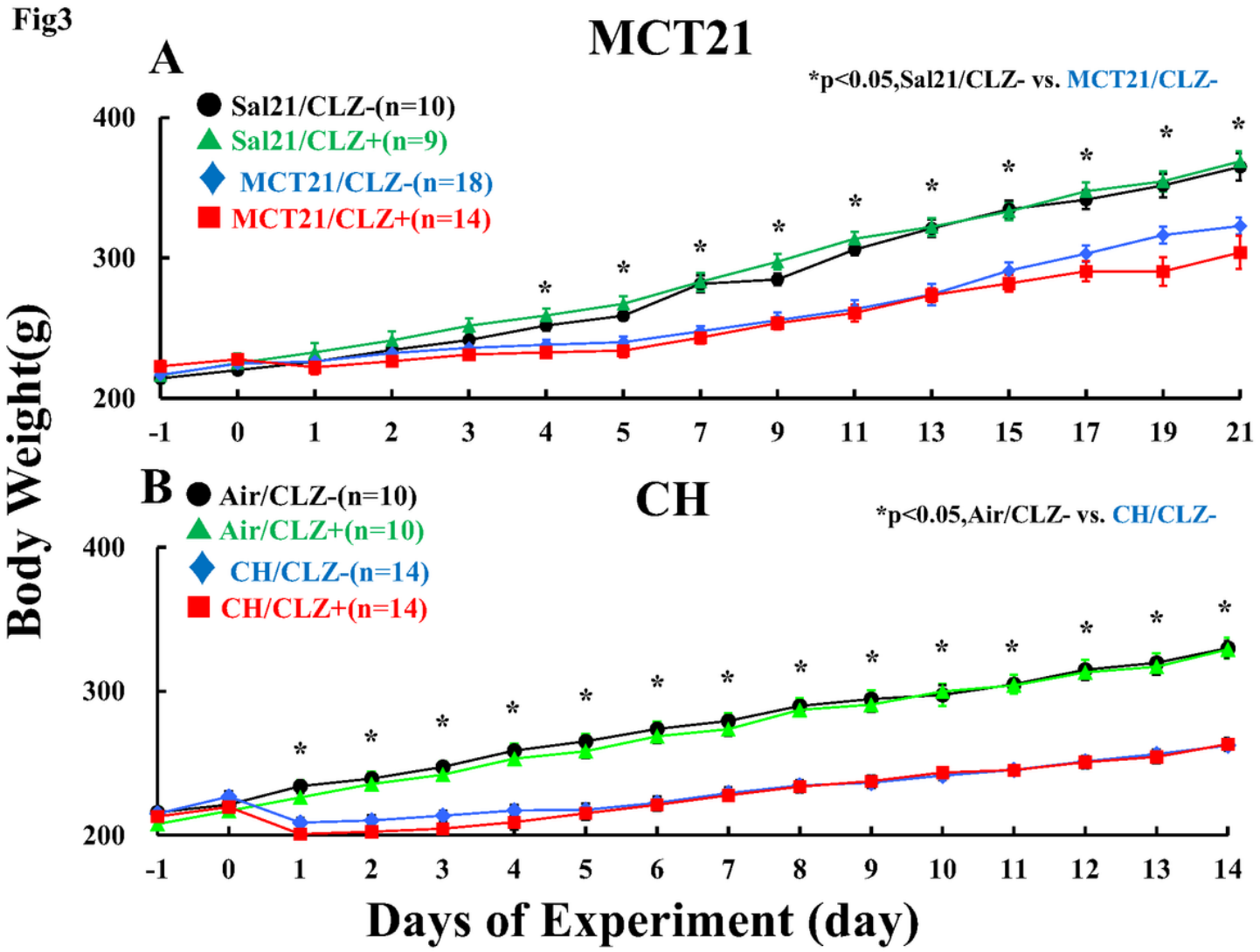

Figure 3

Body weight A Rats injected with monocrotaline (MCT) Sal/CLZ-, rats injected with saline and fed rat chow without cilostazol (CLZ) Sal/CLZ+, rats injected with saline and fed rat chow with CLZ MCT/CLZ-, rats injected with MCT and fed rat chow without CLZ MCT/CLZ+, rats injected with MCT and fed rat chow with CLZ (n)= number of rats, mean ± SE p<0.05, comparison between the Sal/CLZ- group and the MCT/CLZ- group B Rats exposed to chronic hypoxia (CH) Air/CLZ-, rats exposed to ambient air and fed rat chow without CLZ Air/CLZ+, rats exposed to ambient air and fed rat chow with CLZ CH/CLZ-, rats exposed to chronic hypoxia and fed rat chow without CLZ CH/CLZ+, rats exposed to chronic hypoxia and fed rat chow with CLZ (n)= number of rats, mean ± SE p<0.05, comparison between the air/CLZ- group and the CH/CLZ- group

Fig 4

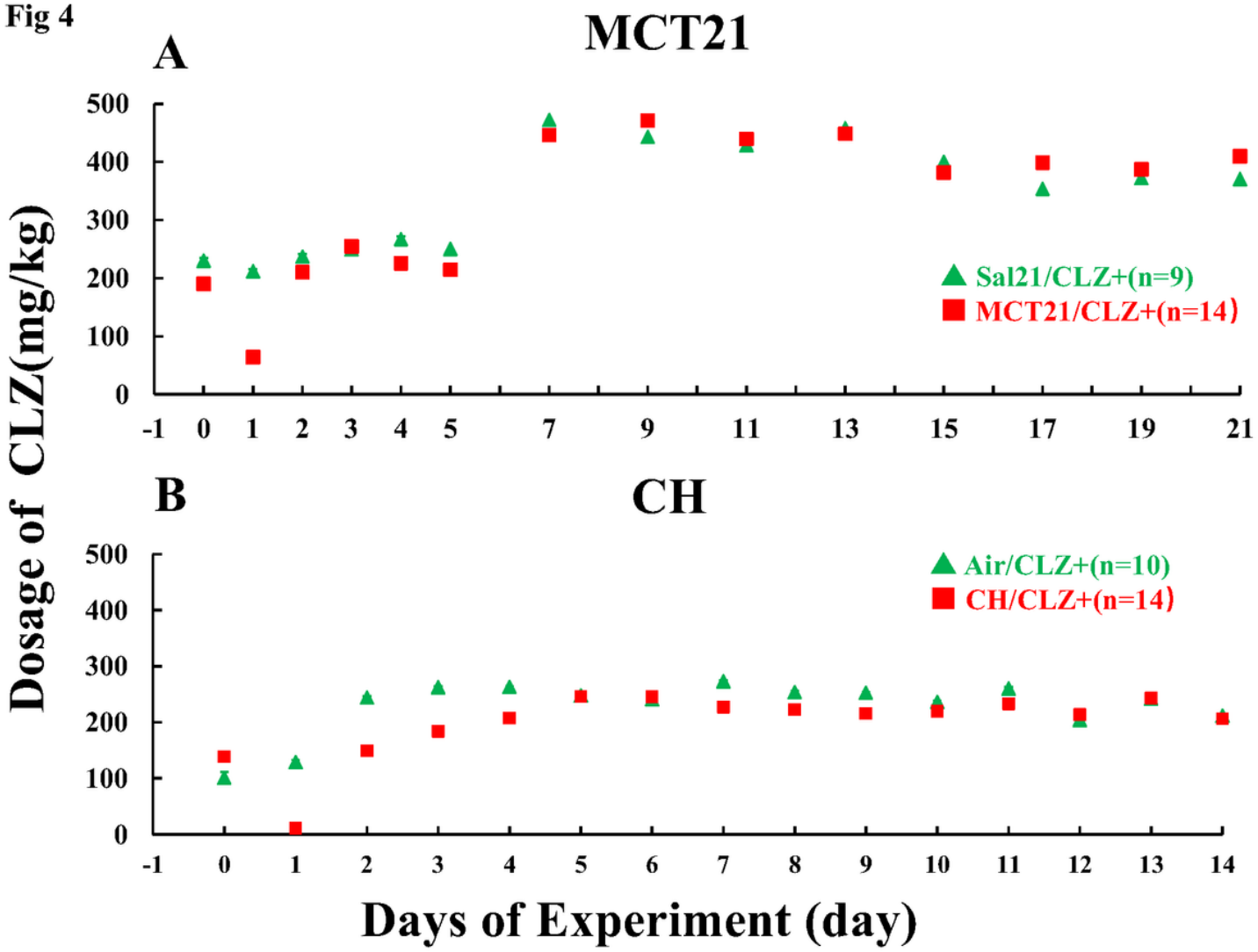

Figure 4

Dosage of CLZ calculated by food intake A Rats injected with monocrotaline (MCT) Each plot is the average dosage per kg per day (from day 0 to day 5) or per 2 days (from day 7 to day 21) for a rat. For example, the plot of day 0 is the dosage a rat had taken for 24 hr from day -1 to day 0, and the plot of day 21 is the dosage a rat had taken for 48 hr from day 19 to day 21. Sal/CLZ+, rats injected with saline and fed rat chow with CLZ MCT/CLZ+, rats injected with MCT and fed rat chow with CLZ B Rats exposed to chronic hypoxia (CH) Each plot is the average dosage per kg per day. For example, the plot of day 0 is the dosage a rat had taken for 24 hr from day -1 to day 0, and the plot of day 14 is the dosage a rat had taken for 24 hr from day 13 to day 14. Air/CLZ+, rats exposed to ambient air and fed rat chow with CLZ CH/CLZ+, rats exposed to chronic hypoxia and fed rat chow with CLZ

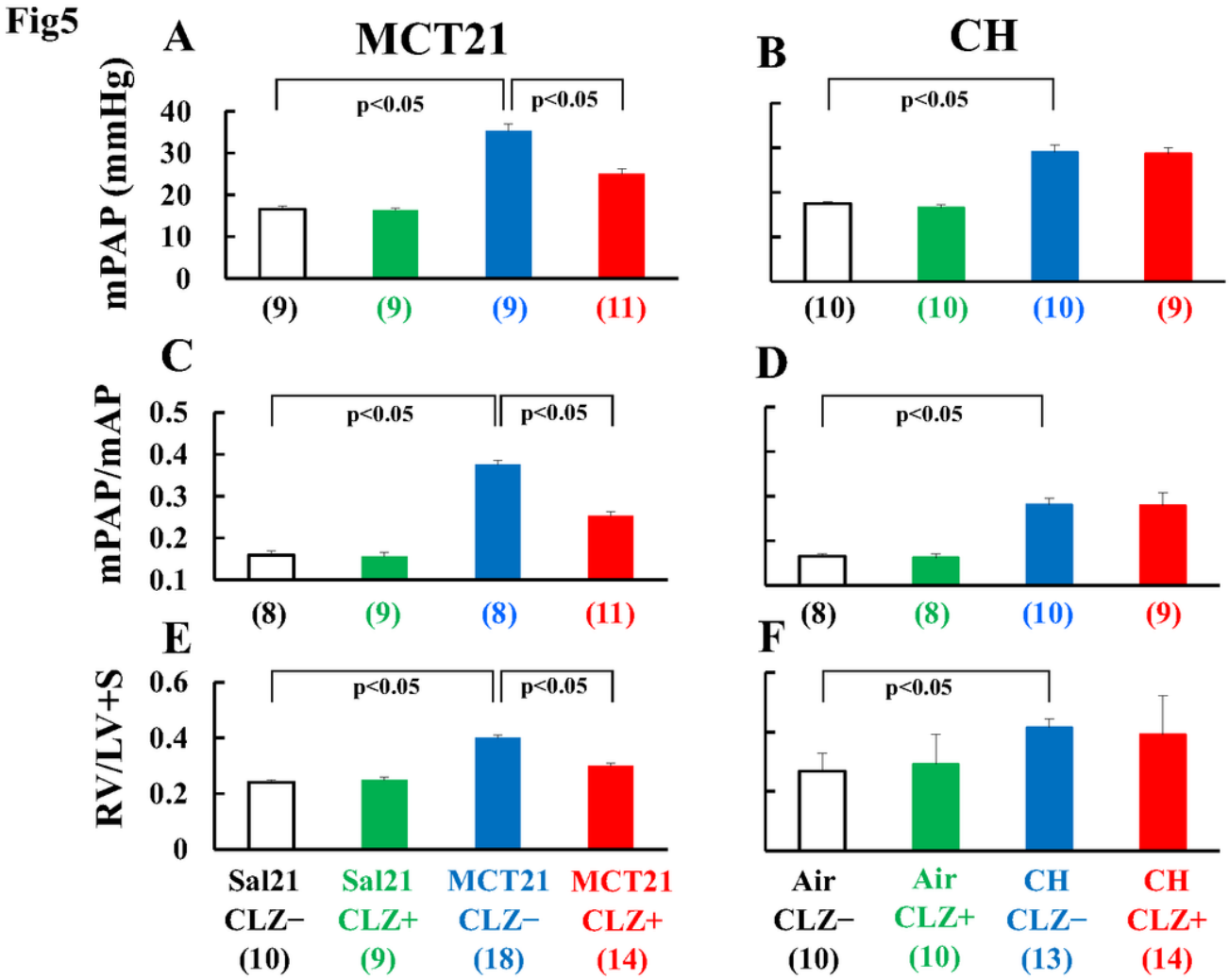

Figure 5

Mean pulmonary artery pressure (mPAP), ratio of mPAP to mean artery pressure (mPAP/mAP), and right ventricle (RV) weight-to-left ventricle+septum (LV+S) weight ratio (RV/LV+S) Left column (MCT21) is in rats in MCT21 model. Right column (CH) shows rats in the CH model (rats exposed to chronic hypoxia for 14 days) CLZ-, fed rat chow without CLZ CLZ+, fed rat chow with CLZ Sal, injected with saline Air, exposed to ambient air for 14 days MCT, monocrotaline; CH, chronic hypoxia (n)= number of rats, mean ± SE The number in parentheses is the number of rats in which mPAP was successfully measured.

Fig6

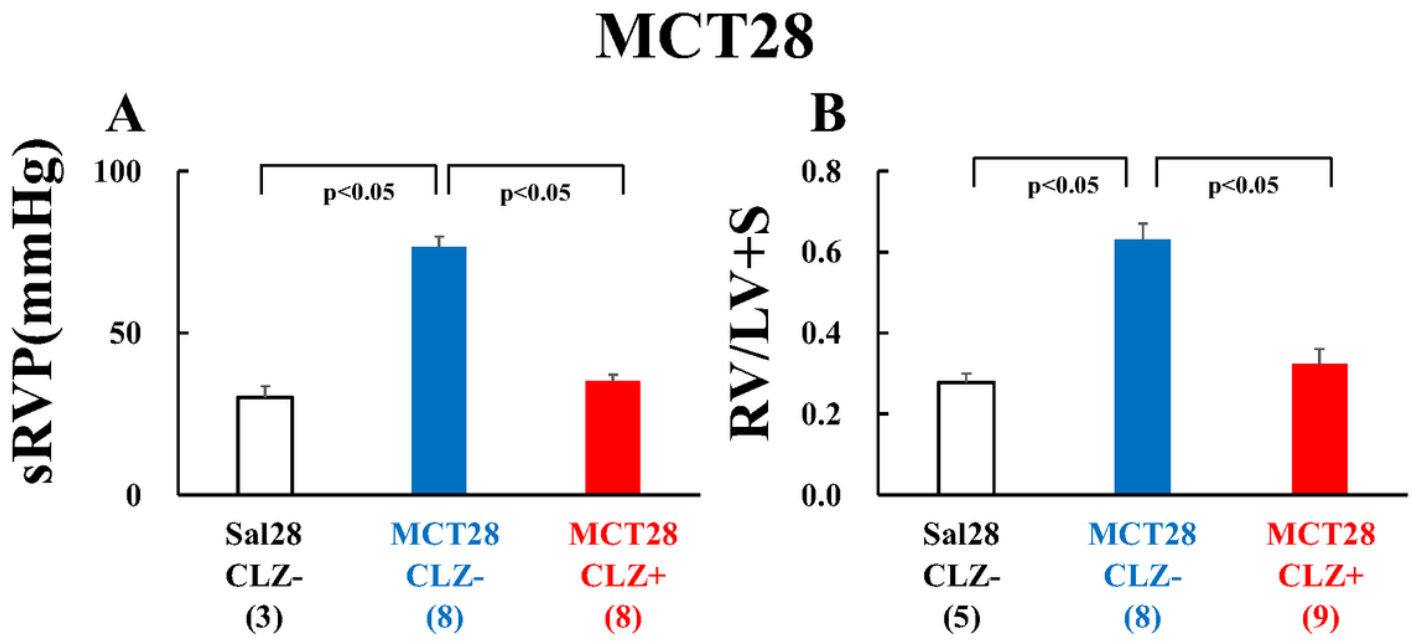

Figure 6

Systolic right ventricular pressure (sRVP) and right ventricle (RV) weight-to-left ventricle+septum (LV+S) weight ratio (RV/LV+S) sRVP under anesthesia and RV/LV+S were measured in rats 28 days after the injection of monocrotaline (MCT28). Sal, injected with saline; MCT, injected with monocrotaline (MCT); CLZ-, fed rat chow without CLZ; CLZ+, fed rat chow with CLZ. (n) = number of rats, mean ± SE

Fig7

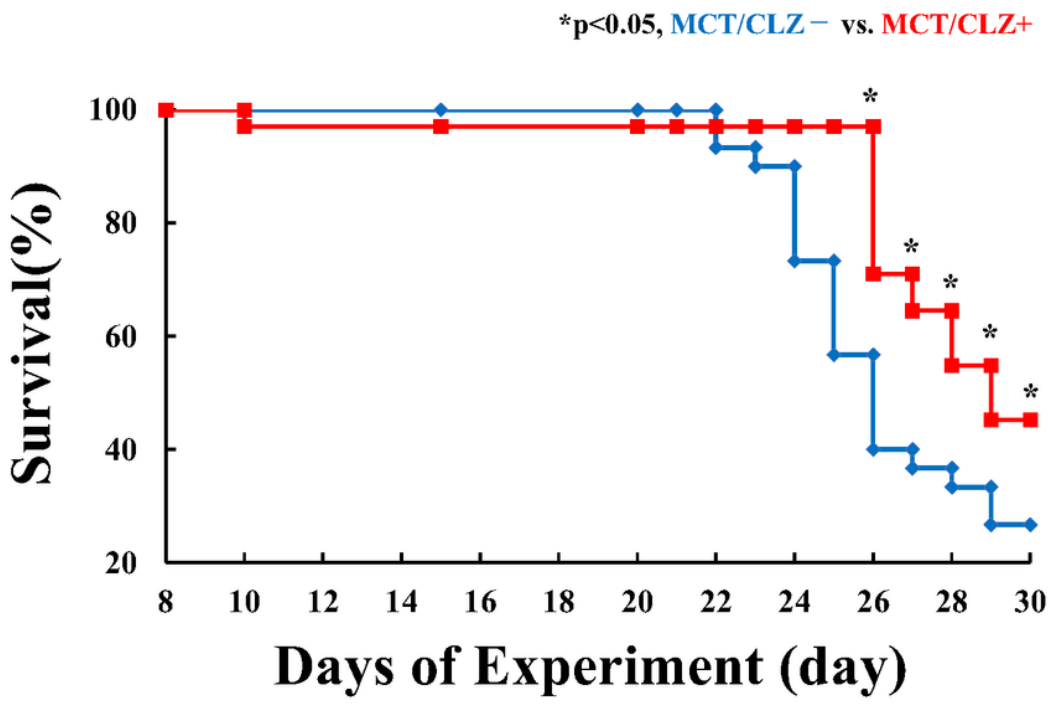

Figure 7

Kaplan-Meier survival curve of rats with and without CLZ treatment after MCT injection Thirty rats with CLZ (MCT/CLZ+) (red line) and 30 rats without CLZ (MCT/CLZ-) (blue line) were used. MCT/CLZ-, rats injected with MCT and fed rat chow without CLZ MCT/CLZ+, rats injected with MCT and fed rat chow with CLZ P<0.05. compared to rats without CLZ

Fig8

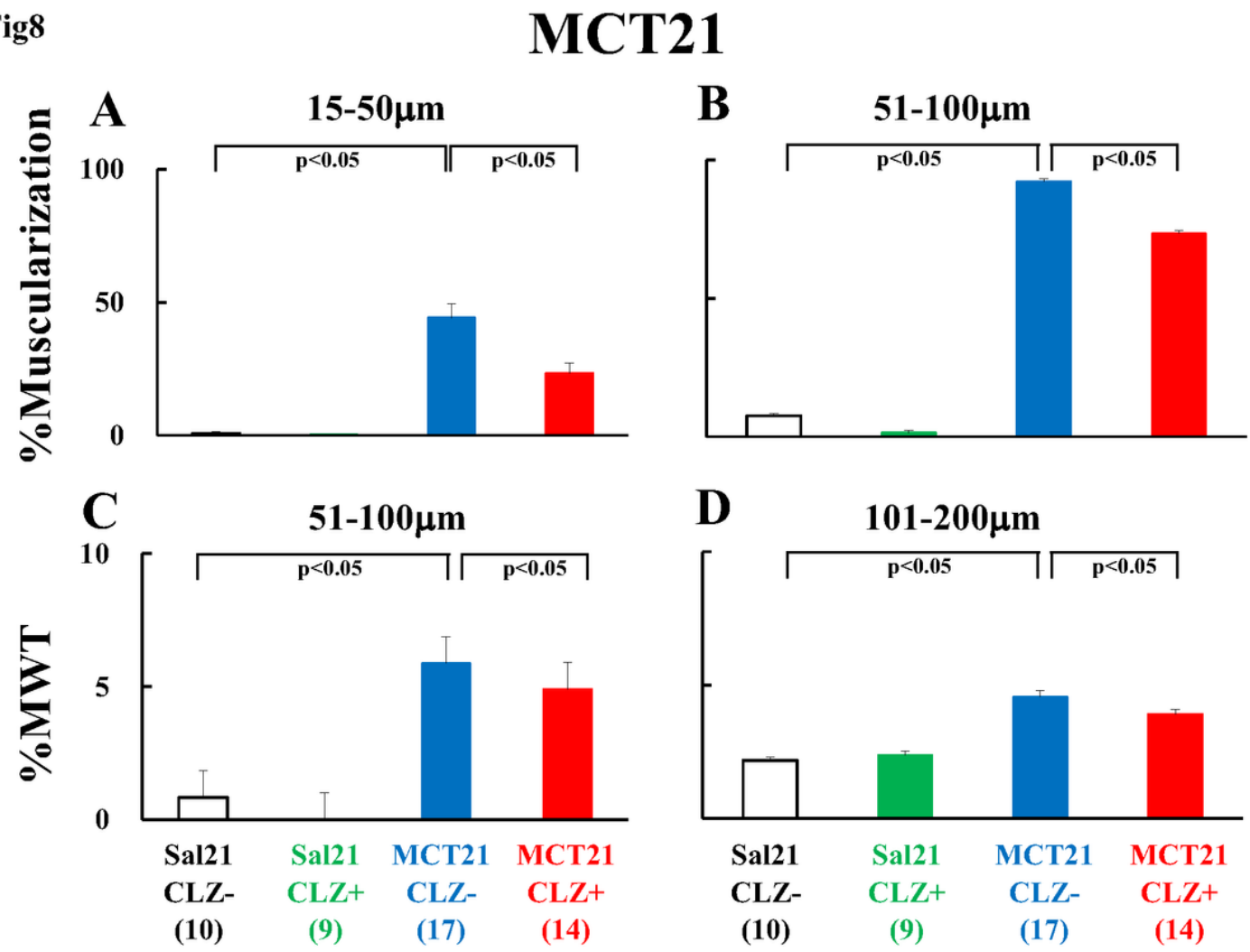

Figure 8

%Muscularization and %MWT in rats injected with monocrotaline (MCT). The data were obtained in MCT21 cells (rats fed with and without CLZ for 21 days after the injection of MCT). %Muscularization, the percentages of muscularized arteries in peripheral pulmonary arteries with an external diameter between 15 and 50 µm (A) and those between 51 and 100 µm (B). %MWT, %Medial wall thickness, is the ratio of the wall thickness of the media (distance between external and internal elastic laminae) to the external diameter in muscular arteries with an external diameter between 51 and 100 µm (C) and those between 101 and 200 µm (D). Sal, injected with saline; MCT, injected with monocrotaline (MCT); CLZ-, fed rat chow without CLZ; CLZ+, fed rat chow with CLZ. (n)= number of rats, mean ± SE

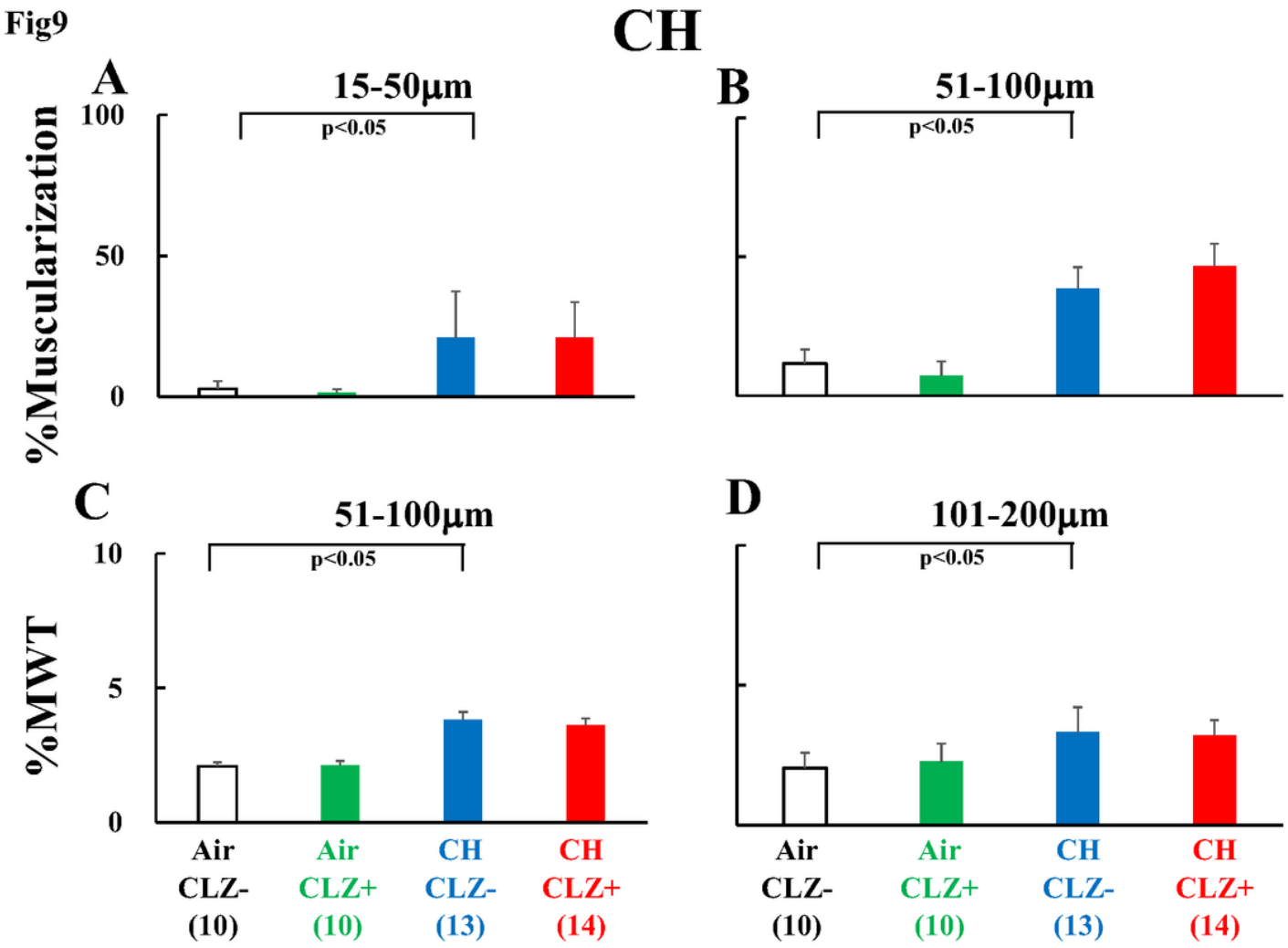

Figure 9

%Muscularization and %MWT in rats exposed to chronic hypoxia The data were obtained in rats exposed to chronic hypoxia (CH) for 14 days. Air, exposed to ambient air; CH, rats exposed to chronic hypoxia; CLZ-, fed rat chow without CLZ; CLZ+, fed rat chow with CLZ. See Figure 6 for other abbreviations

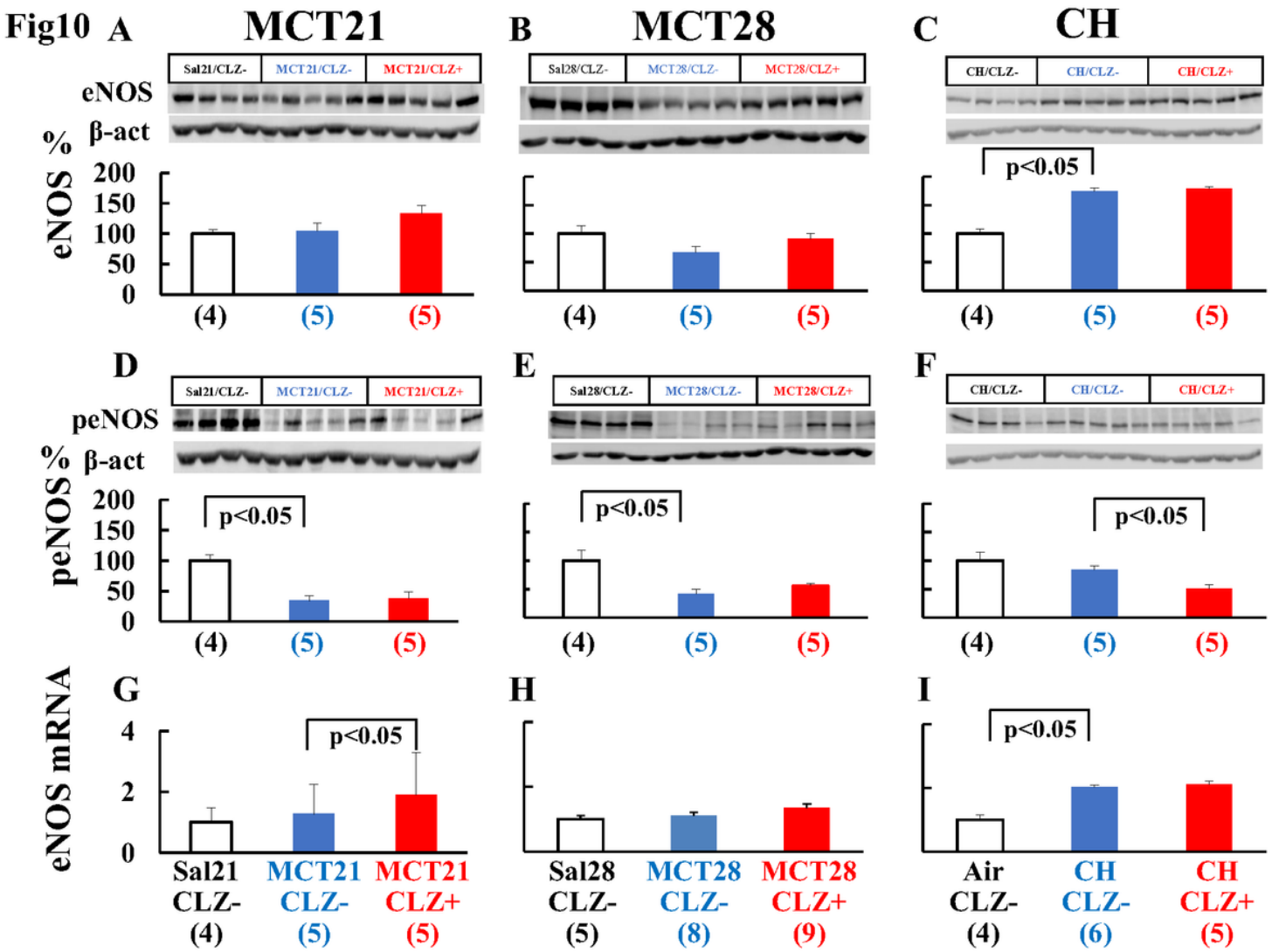

Figure 10

Endothelial nitric oxide synthase (eNOS) and phosphorylated eNOS protein levels and eNOS mRNA Left column (MCT21) is in rats in MCT21 model Middle column (MCT28) is in rats in MCT28 model Right column (CH) is in rats in CH model Representative images of Western blot showed eNOS and peNOS protein. (A, B, C, D, E, F) Sal, injected with saline; MCT, injected with monocrotaline (MCT). Air, exposed to ambient air; CH, rats exposed to chronic hypoxia; CLZ-, fed rat chow without CLZ; CLZ+, fed rat chow with CLZ. The average intensity of Sal/CLZ- in MCT21 and MCT28 cells and Air/CLZ- in CH cells was taken as 100%. Each sample intensity as a percentage of the average value was calculated (relative intensity). (n)= number of rats, mean ± SE

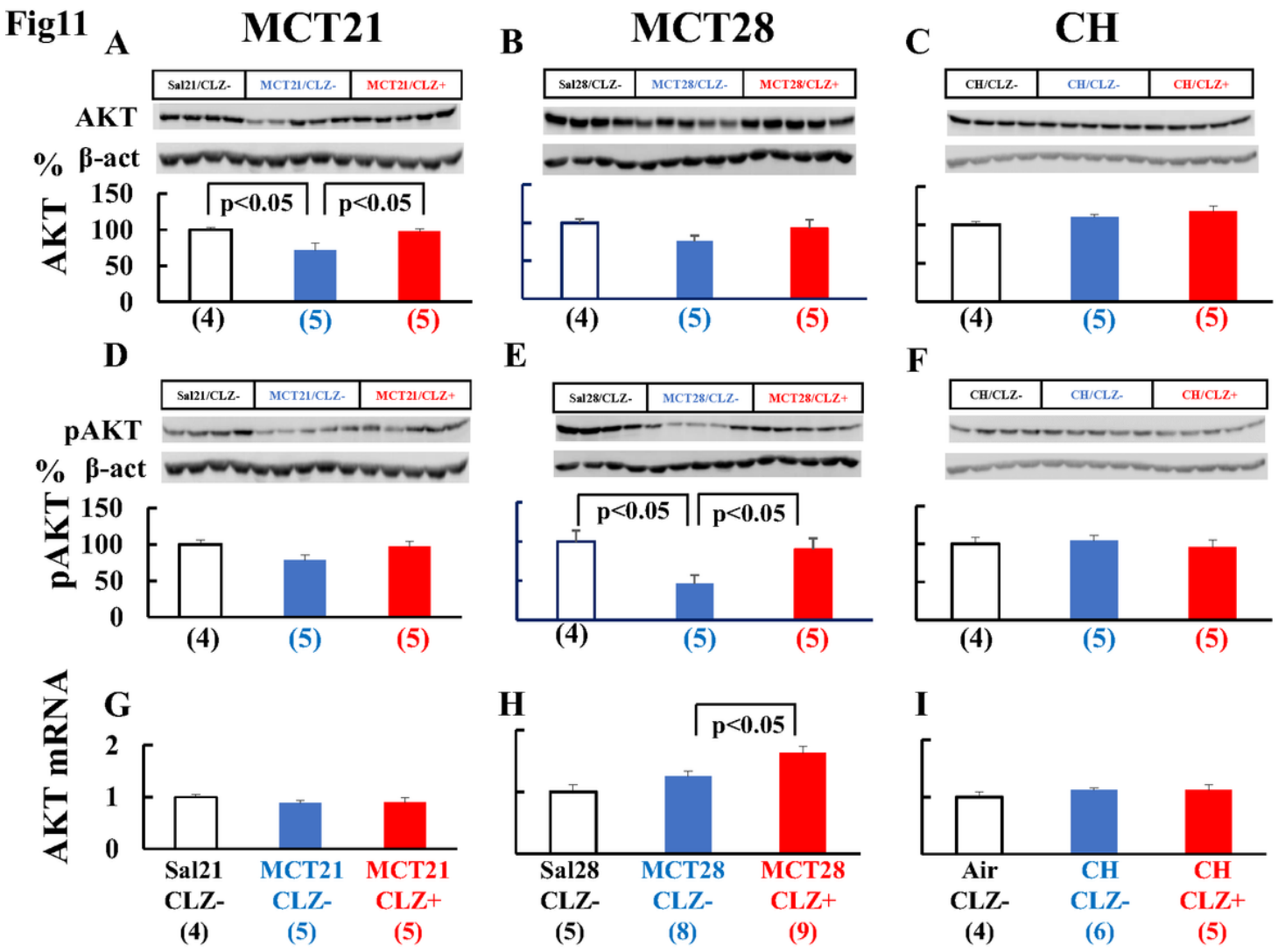

Figure 11

AKT and phosphorylated AKT (pAKT) protein levels and AKT mRNA Representative images of Western blot showed AKT and pAKT protein. (A, B, C, D, E, F) Sal, injected with saline; MCT, injected with monocrotaline (MCT). Air, exposed to ambient air; CH, rats exposed to chronic hypoxia; CLZ-, fed rat chow without CLZ; CLZ+, fed rat chow with CLZ. (n)= number of rats, mean ± SE See Figure 10 for abbreviations.

Fig12

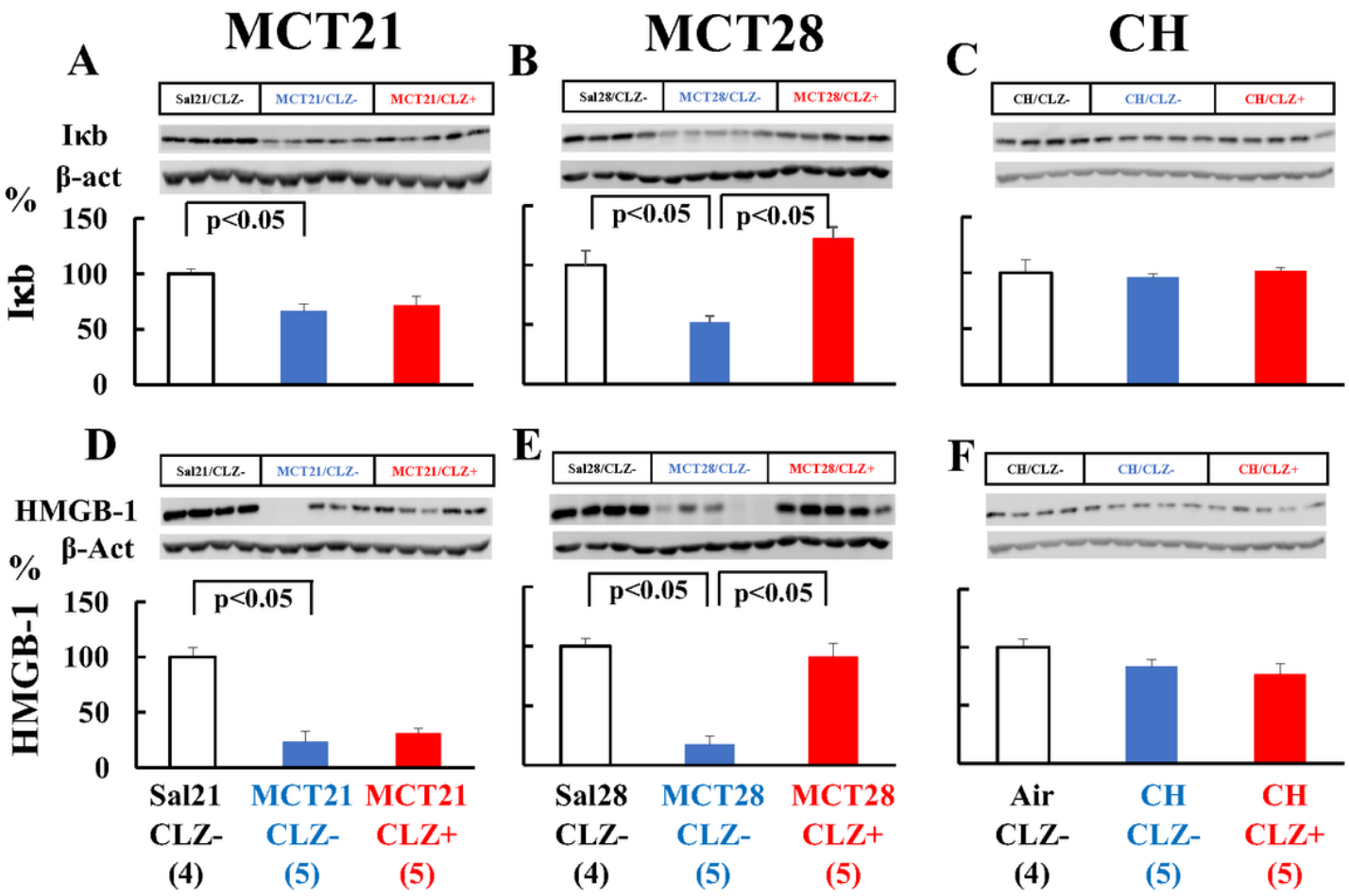

Figure 12

Western blot analysis of IκB and HMGB-1 Representative images of Western blot showed IκB and HMGB-1. (A, B, C, D, E, F) Sal, injected with saline; MCT, injected with monocrotaline (MCT). Air, exposed to ambient air; CH, rats exposed to chronic hypoxia; CLZ-, fed rat chow without CLZ; CLZ+, fed rat chow with CLZ. HMGB1, High-mobility group box-1. (n)= number of rats, mean ± SE See Figure 10 for abbreviations

Fig13

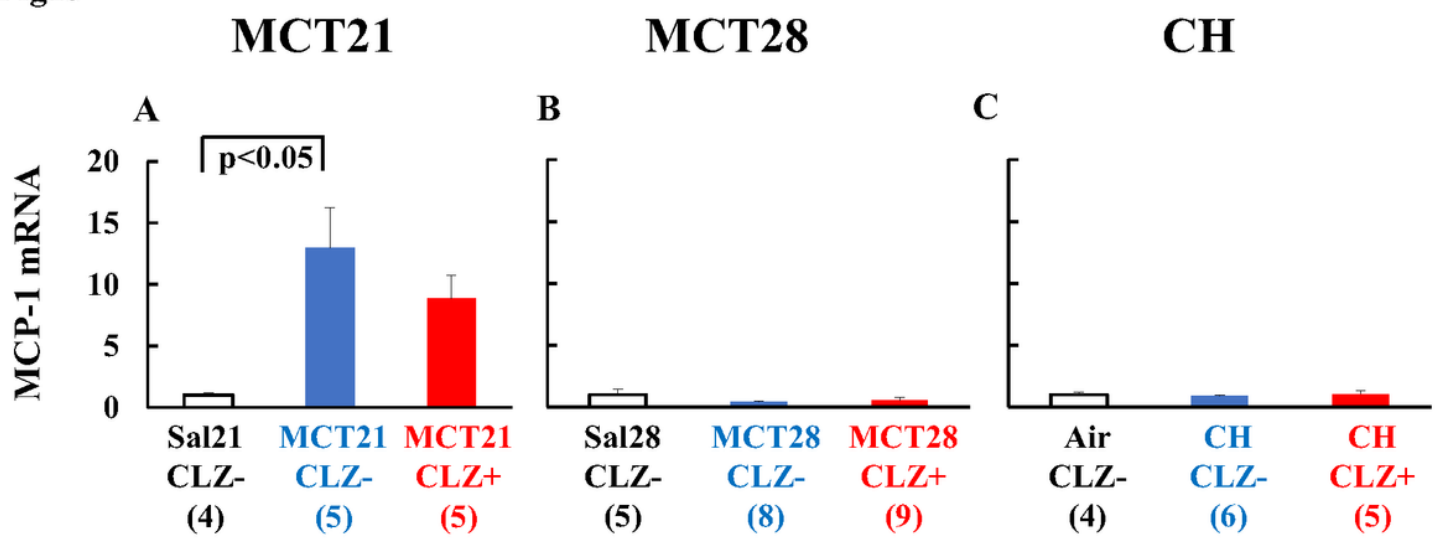

Figure 13

MCP-1 mRNA Sal, injected with saline; MCT, injected with monocrotaline (MCT). Air, exposed to ambient air; CH, rats exposed to chronic hypoxia; CLZ-, fed rat chow without CLZ; CLZ+, fed rat chow with CLZ. MCP-1, Monocyte chemotactic protein-1. (n)= number of rats, mean ± SE See Figure 10 for abbreviations

Supplementary Files

This is a list of supplementary files associated with this preprint. Click to download.

- Table.1.pdf
- AuthorChecklistE10only.pdf
- renamedf9a91.pdf